Eur. Phys. J. D **15**, 365–371 (2001)

THE EUROPEAN PHYSICAL JOURNAL D

EDP Sciences

Non-stationary characteristics of instability in a single-mode Nd:YVO_4 laser with fiber feedback

T.-H. Yang[1], T.-S. Lim[1,a], J.-L. Chern[1], and K. Otsuka[2]

[1] Department of Physics, National Cheng Kung University, Tainan 70101, Taiwan ROC
[2] Department of Applied Physics, Tokai University, 1117 Kitakaname Hiratsuka, Kanagawa 259-1292, Japan

Received 28 March 2001 and Received in final form 5 June 2001

Abstract. Random chaotic burst generation was experimentally observed in a single-mode microchip Nd:YVO_4 laser with fiber feedback. As the feedback strength was increased, a transition from stable relaxation oscillation state to unstable random chaotic burst state appeared. Furthermore, the non-stationary characteristic of probability association was experimentally identified at the transition of the two states while similar characteristics were reported only by numerical simulations of simple dynamical systems. This implies the general feature of non-stationary property of the dynamic switching between two states at transition. The observed chaotic burst generation and non-stationary nature were reproduced numerically based on the Lang-Kobayashi model.

PACS. 42.55.Rz Doped-insulator lasers and other solid state lasers

1 Introduction

Studies on nonlinear dynamics have explored the fundamental mechanisms of the onset of complex phenomena. The dynamic features of such phenomena are usually described by a probability distribution in which a *stationary* assumption is required [1]. By "stationary" we mean that after transient, the probability distribution used to describe the dynamic variable remains the same; "non-stationary" means that the probability distributions behave differently. Non-stationary processes can easily occur due to fluctuations in the control parameters and the characterization of non-stationary properties is of current interest [2]. In deterministic diffusion [3] with a time series $\{x_i\}$, the probability association, which is formed by the connection between $P(\Delta x_k)$ of different k where $P(\Delta x_k)$ $(k = 1, 2, ...)$ is the probability distribution of $\Delta x_k = x_{n+k} - x_n$, can be regarded as a simple way of distinguishing different forms of chaos and their geometric structure in ecological data or biological time series where standard dynamical system theory techniques can not be applied easily. It has been shown that a non-stationary characteristic of probability association exists in chaos. Such a novel characteristic is inherent in dynamic systems at the onset of weak chaos [4]. Furthermore, it has also been shown that a stationary probability distribution $P(\Delta x_k)$ occurs for strong chaos (characterized by a large positive Lyapunov exponent) and a non-stationary distribution for weak chaos (characterized by a positive but small Lyapunov exponent) [5].

In practical systems, delay and/or feedback is inevitable. Dynamics of delayed-feedback systems is of infinite dimensions and it is important to various fields, including physics, chemistry, biology, economics, physiology, neurology, and optical systems. Paradigmatic examples of delayed dynamics are the Ikeda model for optical turbulence in nonlinear optical resonators and the Mackey-Glass model for physiological systems [6]. In the past decades, the instabilities of nonlinear optical resonators and lasers with delayed feedback attracted much attention. A laser diode (LD) with optical feedback has been an attractive system in investigating chaotic dynamic in optics. Optical feedback gives rise to periodic and chaotic oscillations in the laser output power and sometimes leads to internal mode hopping or coherence collapse. One of the unstable features of laser output is low frequency fluctuation (LFF). Recently the LFF was explained theoretically, in the view point of nonlinear dynamics, as the collision between a local chaotic attractor and antimode [7], as a chaotic itinerancy with a drift [8,9], or as a competition between stable and unstable external cavity modes (ECMs) [10].

On the other hand, LD-pumped microchip solid-state lasers exhibit an extremely sensitive response to the external feedback because the photon lifetime τ_S is extremely short compared with the fluorescent lifetimes τ_f [11]. In short, in microcavity lasers with a large lifetime ratio, K $(= \tau_f/\tau_S)$, a large amount of reflected light is introduced into the cavity within the lasing time scale $(\simeq\tau_f)$. Generally, the lifetime ratio of microchip solid-state lasers ranges from 10^5 to 10^7, while $K \simeq 10^3$ in LDs. In fact, in an early experiment on an Ar-laser-pumped microchip LNP ($LiNdP_4O_{12}$) solid-state laser with external

[a] e-mail: tslim@phys.ncku.edu.tw

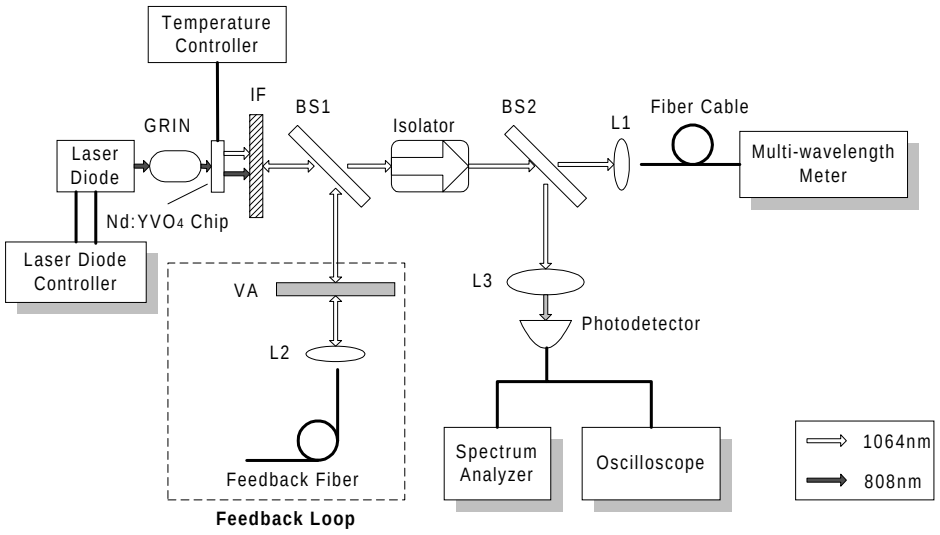

Fig. 1. Experimental setup. L1, L2, L3: lens. BS1, BS2: beam splitter. GRIN: GRIN lens. IF: interference filter. VA: variable attenuator. The solid arrows indicate the 808 nm pumping light from the LD and the empty arrows indicate the 1064 nm laser light from the Nd:YVO_4 laser.

feedback, the random chaotic burst (RCB) instability was observed in a weakly coupled regime, in which two solitary laser modes were involved [12]. A recent more refined experiment indicated that RCB instability is caused by a low-frequency mode-partition noise in multimode LNP lasers [13].

The main objective of this paper is to show that an intriguing non-stationary character of the similarity distribution in peak fluctuation is inherent in a laser system with delayed external feedback. An intensity probability distribution and a probability association analysis of experimental time series are used to evaluate the *non-stationary* property of the laser output. Observed RCB instability and non-stationary characteristics can be well reproduced using Lang-Kobayashi (L-K) equations including intrinsic noise. This paper is organized as follows. In Section 2, experimental setup and the general characteristics of laser output are described. In Section 3, the model of our experimental system, *i.e.*, L-K equations, is illustrated. In Section 4, a simple analysis is provided to indicate the importance of time-step difference analysis, *i.e.*, probability association. The probability association analysis is then detailed. Experimental results are shown in Section 5 and the numerical simulation results based on L-K equations with phase noise are discussed in Section 6. We finally conclude our work in Section 7.

2 Experimental setup and general characteristics

To give a clear picture of our experimental observation we provide the details of experimental setup as follows. The schematic diagram of the experimental setup is shown in Figure 1. The experiment was carried out by utilizing a typical LD-pumped microchip neodymium doped yttrium orthovanadate (Nd:YVO_4) laser. The Nd:YVO_4 laser crystal, which is commercially available from the CASIX Inc. (CASIX DPO3104), is 1 mm thick and 1% Nd^{3+} doped. By specification, the output coupling was 5±2% at 1064 nm.

Since fluctuation is crucial to the results, Nd:YVO_4 laser chip was stuck on a 2 mm thick copper mount and its temperature was kept at 22 °C to reduce thermal fluctuation by a temperature controller (ILX LTD-5910B). A noise filter (ILX 320) was used to eliminate the pumping noise from the current driver. In the mean time, the high power LD (HPD1010-C; lasing wavelength: 808 nm) was driven by a low noise LD controller (ILX LDC-3744). An interference filter was also used to reduce the effect of pumping light on detection.

The pumping beam from the LD was focused onto the laser crystal with a GRIN lens (0.22 pitch). The pumping threshold was 40 mW and in the entire pumping domain, laser output was in $\pi-$polarized TEM_{00} mode. The light emitted from the laser was divided into two by a beam splitter plate (CASIX FBS0404). One of the beams was for measurement and the other was for feedback. The feedback strength κ is calculated by the following formula [14],

$$\kappa = \frac{1-R_{\rm m}}{\tau_{\rm L}} \left(\frac{\eta}{R_{\rm m}}\right)^{1/2}, \qquad (1)$$

where $\tau_{\rm L}$ is the cavity round-trip time and is about 1.33×10^{-11} s for an 1 mm thick Nd:YVO_4 chip (the index of refraction: $n_{\rm o}=1.9573$), η is the feedback fraction, and $R_{\rm m}$ is the facet reflectivity of the laser. The onset of instability, the RCB, is confirmed to be caused by feedback. Without feedback, the laser output shows a typical relaxation oscillation (RO). In feedback path, the laser light was coupled into a 10 m single mode fiber (Newport F-SY) and was reflected back to the laser from the open end of the fiber. To control the feedback strength more precisely a variable attenuator (Newport 50G20) was inserted into the feedback loop. For large attenuation, *i.e.*, less feedback light, the laser behaves as a solitary laser. For small attenuation, *i.e.*, more feedback light, the laser output exhibits the RCB instability. However, the feedback is still very weak. The reduction of threshold caused by feedback

light was less then 1% (the solitary laser threshold was 40 mW and the laser threshold with feedback was around 39.8 mW).

In measurement, a multi-wavelength meter (HP 86120B) was used to monitor the variation in lasing mode. The single mode operation maintained from threshold to 110 mW pumping power. The lasering wavelength was 1064.245 nm. To prevent laser light to be fed back from the measurement part, an isolator (ISOWAVE I-106-2L) was utilized. We used a low-noise detector (New Focus 1611) to detect the laser output. The ac and dc ports of the detector were connected to a transient oscilloscope (HP 54542C) for data acquisition and a spectrum analyzer (HP 8591E) for power-spectrum analysis.

All experimental results were obtained for a fixed pumping power of 88 mW. Although the results presented are for a pumping power of 88 mW, the features we identified are generic for all the single-mode region. In the absence of fiber feedback, the laser output exhibited small-amplitude RO driven by white noise and the relaxation oscillation frequency (f_{RO}) was about 1.5 MHz. As the pumping power was varied, f_{RO} increased following the relation, $f_{\mathrm{RO}} \propto \sqrt{(W-1)/(\tau_{\mathrm{S}}\tau_{\mathrm{f}})}$, where $W = P/P_{\mathrm{th}}$ is the normalized pumping power and P and P_{th} are the pumping power and the threshold pumping power respectively. The fluctuation in the ac part was around 20 mV, while the dc value was about 150 mV.

The optical power injected into the fiber was estimated to exceed 3 mW. As feedback strength was increased to exceed $220\tau_{\mathrm{f}}^{-1}$, assuming $\tau_{\mathrm{f}} = 90$ μs, the RCB occurred. A typical temporal waveform of the RCB is shown in the lower graph of Figure 2 for $\kappa = 375\tau^{-1}$. Here, the sampling rate of the oscilloscope is 100 MHz. There are two kinds of waveform in the graph. One waveform is the small amplitude fluctuation waveform as shown in the left portion of the graph. The upper graph of Figure 2 shows the corresponding result of the joint time-frequency analysis (JTFA) used to explore the dynamics. The analysis here is based on the short-time Fourier transform with the Hanning window. The window length is 512 samples, *i.e.*, 5.12×10^{-6} s. The time interval of each window is 128 samples, *i.e.*, 1.28×10^{-6} s. As shown in the left portion of the graph, the laser output intensity oscillates at a frequency of about 1.5 MHz and its high order harmonics can be recognized. This is just the main feature of noise-driven RO. As time evolved, a different kind of waveform, spike oscillation waveform, was observed as shown in the right portion of the lower graph in Figure 2 and the waveform has been identified to be a chaos based on the singular value decomposition analysis [15]. As shown by the JTFA, the main frequency component shifts to about 1 MHz and a broad-band characteristic appears as shown in the right portion of the upper graph. The insert of the lower graph of Figure 2 shows a longer temporal waveform. As the figure shows, the laser output randomly switches between these two kinds of waveform. Note that the basic characteristics of the dynamical transition between two waveforms features a broadening in the rf spectrum. In transition region, the rf spectrum broadens gradually and the main frequency component shifts downward as shown in the center portion of the upper graph in Figure 2.

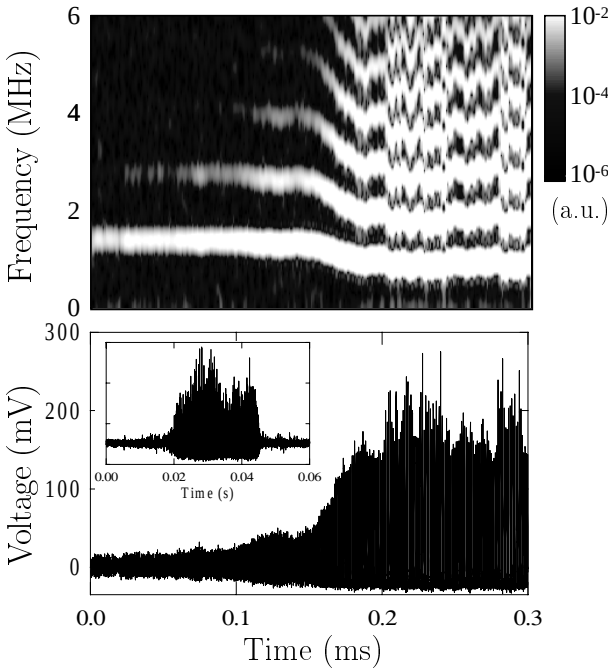

Fig. 2. General characteristic of the RCB. The lower graph is the typical temporal waveform of the RCB and the upper graph is the corresponding the JTFA spectrum. The level of power spectrum estimate is denoted by the gray level of color. The insert shows a longer temporal waveform. Here, $\kappa = 375\tau_{\mathrm{f}}^{-1}$.

To sum up, the Nd:YVO_4 laser emits two kinds of output under different feedback strengths. From $\kappa = 0$ to $\kappa = 220\tau_{\mathrm{f}}^{-1}$, the laser output exhibits a noise-driven RO output and is named as the RO state. When $\kappa > 220\tau_{\mathrm{f}}^{-1}$, the laser output randomly switches between the RO waveform and the spike oscillation waveform. This is named as the RCB state. Laser output exhibits different dynamical significance in these states as to be further illustrated below.

3 Laser model description

The issue of instabilities in the output of lasers which are subjected to external feedback was initiated by the pioneering work of Lang and Kobayashi in 1980 [16]. They demonstrated the dynamical instabilities in a LD with external feedback which feature sustaining relaxation oscillations. They also confirmed theoretically that the dynamical instabilities take place in the transition process where the lasing frequency changes from one ECM to another in a weak-coupling regime. Since our system is essentially a single-mode laser with weak feedback, we used the following normalized L-K model [16] with Langevin noise

sources [17] to explore the dynamics.

$$\mathrm{d}S(t)/\mathrm{d}t = K\{[N(t)-1]S(t)\} + 2\kappa\sqrt{S(t)S(t-T)}\cos\theta(t) + F_S(t), \quad (2)$$

$$\mathrm{d}N(t)/\mathrm{d}t = W - N(t) - N(t)S(t) + F_N(t), \quad (3)$$

$$\mathrm{d}\phi(t)/\mathrm{d}t = (\omega_0 - \omega_{\mathrm{th}}) + \frac{\alpha}{2}K[(N(t)-1] - \kappa\sqrt{S(t-T)/S(t)}\sin\theta(t) + F_\phi(t), \quad (4)$$

where $S(t)$ is the normalized photon density, $N(t)$ is the normalized population inversion density, $\phi(t)$ is the phase shift, T is the delay time, α is the linewidth enhancement factor, ω_0 is the lasing-mode angular frequency, ω_{th} is the lasing-mode angular frequency near threshold without feedback, and $\theta(t) = \omega_0 T + \phi(t) - \phi(t-T)$ is the phase difference between the output and feedback beams [14]. The t and T have been normalized with τ_{f}. To simulate the experimental observation, we introduced the Langevin noise terms into the L-K equations: F_S, F_N, and F_ϕ for S, N, and ϕ, respectively. Here, $\langle F_i(t)\rangle = 0$ and $\langle F_i(t)F_j(t')\rangle = 2D_{ij}\delta_{ij}\delta(t-t')$, where $i = S$, N, and ϕ. Here, $\langle . \rangle$ denotes time average.

Equations (2–4) would be reduced to a set of typical class-B laser rate equations for S and N only, as $\kappa = 0$. With these two equations, the system is essentially stable, *i.e.*, no instability could be observed without introducing any additional degree of freedom. For a nonzero κ, the dynamical behaviors of the equations become very complex and instability is possible to happen depending on the parameters. As mentioned above, the laser output exhibits different behaviors, *i.e.*, noise-driven RO and RCB, under different κ. The statistic characteristics of the laser output in each case are supposed to be different. In the following discussion, we will take the peak values of the laser output and perform the statistic analysis.

4 Probability association analysis

To identify the transition from the RO state to the RCB state more clearly, we evaluated the mean and the standard deviation values of the peak intensities at different coupling strengths. Using the digital oscilloscope, we repeatedly accumulated the time series of the laser output and identified the discrete peak values, $S_{p,n}$, where S_p is the peak of laser output and n denotes the nth peak. To obtain a reliable probability, a total of 320 000 peaks were collected at each specific rotation angle of the attenuator (*i.e.*, the feedback strength). Asymptotically, as $\kappa \to 0$, the system features a free-running laser such that the mean and the standard deviation values of S_p are small. For larger κ, due to the appearance of chaotic spiking waveform, the mean values of S_p should become large. In the meantime, due to the random switch between the RO waveform and the chaotic spiking waveform, the standard deviation values of S_p should be also large. Figure 3 shows the mean and standard deviation values of S_p as a function of feedback strength κ. Indeed, small mean values and standard deviation values feature the RO state

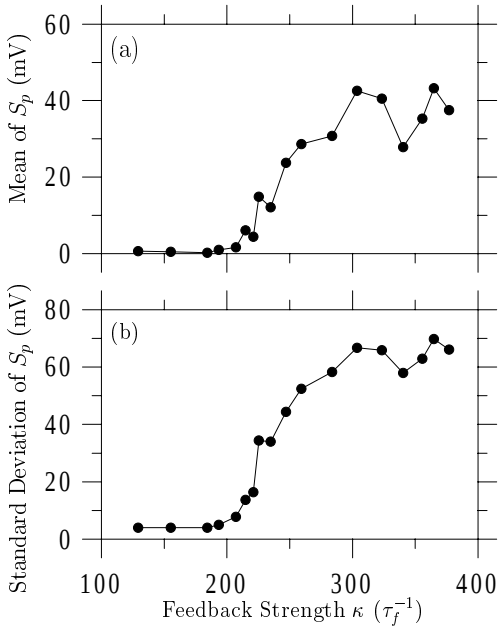

Fig. 3. (a) The mean values and (b) the standard deviation values of S_p as functions of κ.

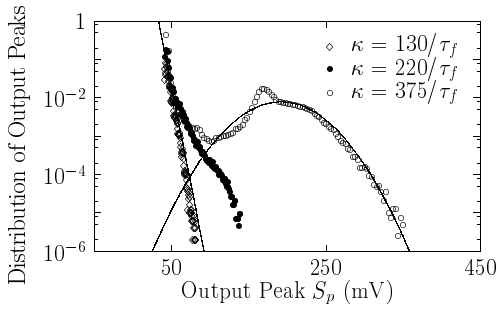

Fig. 4. Probability distribution of experimental peak intensities S_p at $\kappa = 130/\tau_{\mathrm{f}}$ ($\diamond$), $\kappa = 220/\tau_{\mathrm{f}}$ ($\bullet$), and $\kappa = 375/\tau_{\mathrm{f}}$ ($\circ$). Two solid lines are the fitting curves in the form of $a_0 \mathrm{e}^{a_1 S_p}$ and $b_0 \mathrm{e}^{b_2 (S_p - b_1)^2}$.

in the small κ regime and large mean values and standard deviation values feature the RCB state in the large κ regime. There is a dramatic increase in both mean and standard deviation values at a feedback strength of around $\kappa = 220\tau_{\mathrm{f}}$, which implies the onset of the RCB instability.

Next, we calculated the probability distribution of the peak intensity for different feedback strengths. In the RO state, which exhibits noise-driven RO, the probability distribution of the peak power, $P(S_p)$, followed an exponential law and featured shot-noise characteristics as shown by the empty diamond symbols in Figure 4. However, by increasing the feedback strength, a tailed probability distribution was created, as shown by the filled circle symbols in Figure 4. Focusing on the time domain in which large-intensity spike oscillations dominated, a Gaussian distribution is seen, as shown by the open circle symbols in Figure 4. This indicates that there are two dynamical states

that follow different statistics (*i.e.*, shot-noise characteristics and Gaussian distribution, as indicated by the two solid fitting lines, which are in the form of $a_0 e^{a_1 S_p}$ and $b_0 e^{b_2 (S_p - b_1)^2}$ respectively, in Fig. 4). They are mixed in the RCB state, yielding a tailed probability. By a joint probability analysis similar to that used in reference [18], such a mixed distribution which implies that there is still a strong overlapping between two probability distributions can be identified. This suggests that the interplay between two states may be rather unique where the statistics on time-difference should be crucial.

From the point of view of a stochastic process, the introduction of a probability distribution to chaos means that a variable, *e.g.*, x_n, can be described as if it were generated by a "random" number generator with a certain probability distribution. In terms of the probability distribution, the connection between two variable x_{i+k} and x_i, which are associated with each other with a k time step difference, is

$$x_{i+k} = x_i + \xi_{,k}, \tag{5}$$

in which $\xi_{,k}$ is a number from a probability distribution $P(\xi_{,k})$, when the value i is chosen arbitrary. The connection between $P(\xi_{,k})$ of different k forms a probability association. For stochastic systems and some common types of chaos, there is a limit for $P(\xi_{,k})$ as $k \to \infty$. However, this feature is not always true as shown in reference [4] that a non-stationary property does exist in some systems. This non-stationary probability feature indicates some novel statistical characteristics of the quantities with time difference in chaos.

Explicitly, as illustrated in reference [4], the analysis was performed as follows. In the beginning, we accumulated a long enough time series of the peaks of laser output, $\{S_{p,n}\}$, $n = 1, ..., N'$, after the transient. Similar to the consideration applied to deterministic diffusion or just because the memory of the initial conditions will be lost as the time difference increases, we looked at the dynamic behavior of a $k-$step difference quantity, *i.e.*,

$$\Delta S_{p,k} = S_{p,k+l} - S_{p,l}, \tag{6}$$

rather than $S_{p,l}$ itself. Here l can be $1, 2, ..., N (N < N')$. The maximum and the minimum of $\Delta S_{p,k}$ can be determined. We further divided the range of $\Delta S_{p,k}$ into M intervals according to the resolution ability we have. We can count the numbers of $\Delta S_{p,k}$ appearing in each interval. After dividing these numbers with the total number N, we derived a probability distribution $P(\Delta S_{p,k})$ of $\Delta S_{p,k}$. Next we investigated the "association" of two probability distributions, *i.e.*, $P(\Delta S_{p,k+j})$ and $P(\Delta S_{p,k})$, by calculating a χ^2 which is defined as

$$\chi^2(j;k) = \sum_i^M \frac{(R_i - S_i)^2}{(R_i + S_i)}, \tag{7}$$

where R_i and S_i are the probabilities of the ith interval for $P(\Delta S_{p,k+j})$ and $P(\Delta S_{p,k})$, respectively. The summation was carried out for all intervals except $R_i = S_i = 0$. In this paper, we set $j = 1$. Obviously, two similar probability distributions result in a small χ^2. If the two probability distributions differ very much, we get a large χ^2. This is much like the so-called chi-square statistics [19]. The evolution of the association of probability distributions can be described by $\chi^2(j;k)$, as k is varied. This χ^2 is our main characterization tool.

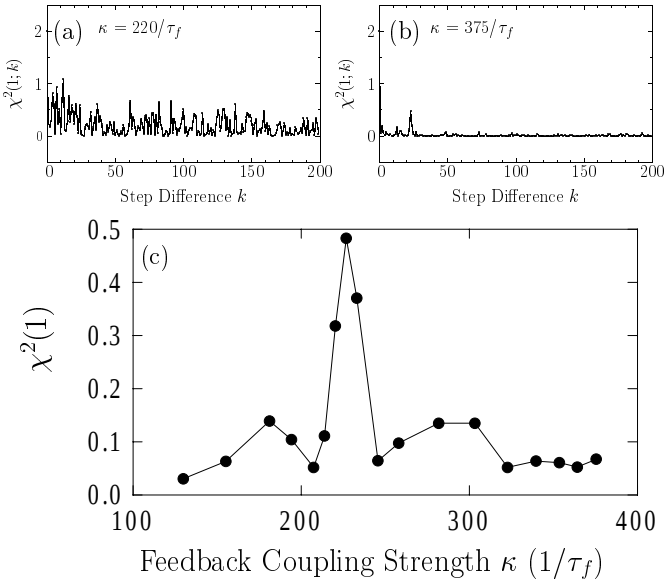

Fig. 5. $\chi^2(1;k)$ for (a) $\kappa = 220\tau_{\rm f}^{-1}$ and (b) $\kappa = 375\tau_{\rm f}^{-1}$. (c) $\chi^2(1)$ at different κ based on experimental data.

5 Experimental results

In the experiment, we calculate $\chi^2(1;k)$ for $k = 1, 2, ..., 200$ and take the average value of these 200 $\chi^2(1;k)$ to be $\chi^2(1)$. Figure 5c shows $\chi^2(1)$ as a function of κ. $\chi^2(1)$ values are almost zero for small κ, *i.e.*, the RO state. The interesting point is that $\chi^2(1)$ value peaked at $\kappa \sim 220\tau_{\rm f}^{-1}$, which corresponds to the transition point referring to Figure 3. Note that at transition the probability distribution drastically changes from the shot-noise character to a tailed distribution. This shows that the transition is associated with a non-stationary characteristic, so successive changes in similarity occur wildly. At a larger feedback strength, *i.e.*, the RCB state, $\chi^2(1)$ becomes small again. Although the mean and the standard deviation values are large due to the chaotic spike burst in this regime and the laser output is of instability for small time scales, the statistic character is unstable for large time scales. This peculiar feature is due to the fact that the increase in feedback strength causes longer staying times in any of the two states (*i.e.*, the noise-driven RO and the chaotic spiking oscillation) before the random switches taking place. As a result, the successive changes in similarity became small. This transition has been found to occur at the same feedback strength independently of the total number of peaks point employed for calculation.

Figures 5a and 5b present $\chi^2(1;k)$ for different k near and after the transition. As shown by Figure 5a, $\chi^2(1;k)$ near the transition never goes to zero, which suggests that the instability has a strong non-stationary nature. On the other hand, after transition, the $\chi^2(1;k)$ is almost zero as shown in Figure 5b. Besides, κ can be transferred to the effective coupling parameter $C = \kappa T\sqrt{1+\alpha^2}$ such that the criterion for the existence of only one ECM, *i.e.*, $C < 1$, can be justified [14]. Here, we should emphasize that when we are measuring some physical properties, such as mean and standard deviation values as shown in Figure 3, we assume the experimental system is stationary, *i.e.*, all parameters of the studied system relevant for its dynamics are fixed and constant during the measurement period, in advance. This is true for most of the physical systems. However, in some physical systems, this can't be true. Nevertheless, the stationary/non-stationary property could be characterized by the probability association analysis. In our experimental system, a stationary to non-stationary nature is well characterized by $\chi^2(1)$ and that the *weak*-feedback-induced instability in the present system is associated with *wild* and *non-stationary* successive changes in the similarity of the variation probability distributions. Similar instability has been observed for various fiber lengths (3, 4, 5, 7, and 100 m). In addition, the instability was observed independently of the pump power level in the regime of single-mode operation.

6 Numerical results

We explored the observed instability by simulating the L-K model, assuming relevant parameters of the microchip Nd:YVO_4 laser with fiber feedback: $W = 1.3\tau_{\rm f}^{-1}$, $K = 2\times10^5$, $\alpha = 1$, $\omega_{\rm th} = 1.6\times10^{11}$ rad$\tau_{\rm f}^{-1}$, and $\kappa = 5\tau_{\rm f}^{-1}$. In this case, only one single ECM solution was obtained as the steady-state solution of equations (2–4). The system presents either stable output or periodic spiking, depending on $\omega_{\rm th}$, in the absence of noise. When a phase fluctuation (*i.e.*, the white Gaussian FM noise) was introduced into $\omega_{\rm th}$, the RCB state could be easily reproduced as shown by the inset in Figure 6, where $D_{SS} = D_{NN} = O(\epsilon)$ ($\epsilon \ll 1$ is the spontaneous emission coefficient) and $D_{\phi\phi} = 7.5$ rad$^2\tau_{\rm f}^{-2}$ were assumed. The excellent agreement between the experimental and numerical results is considered to the result of an FM-noise expected in the Nd:YVO_4 laser [13,20].

The result of probability association analysis based on $\chi^2(1)$ statistics is also shown in Figure 6. A non-stationary characteristic at the transition point, $\kappa \sim 3.3/\tau_{\rm f}$, featuring a large $\chi^2(1)$, can be seen. This agrees with the experimental results shown in Figure 5. In numerical results, the onset point of the instability varies when the parameters, such as α, K, and $\omega_{\rm th}$, vary. However, the non-stationary feature at transition persists.

A similar onset of transition was reproduced numerically with different fiber lengths and pumping powers, where the RCB state appeared with a smaller FM noise when the feedback length (external cavity mode spacing) was increased (decreased). In the case of 10 m fiber

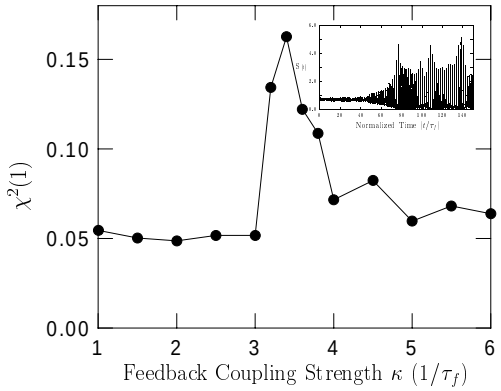

Fig. 6. Typical numerical simulation result of $\chi^2(1)$ for different κ. A typical temporal waveform of the RCB due to the feedback is inserted above.

feedback, for example, the frequency fluctuation of a few MHz in the solitary laser resulted in the RCB state. This matches quite well with a linewidth of 2 MHz measured by a high-resolution scanning Fabry-Perot interferometer.

7 Conclusions

In conclusion, we have clarified the *non-stationary* nature in a single-mode microchip Nd:YVO_4 laser with weak feedback. The non-stationary character was found to be greatly pronounced at a particular feedback strength (*i.e.*, transition point) at which switching from the RO state to the RCB state takes place. In the meantime, our simulations based on the Lang-Kobayashi model with FM noise have reproduced the RCB state. Furthermore, non-stationary nature and the existence of the transition point can be numerically identified.

The non-stationary feature of probability association has been found in some simple nonlinear dynamic systems numerically as shown in references [4,5]. Such a non-stationary feature is inherent in dynamic systems at the onset of weak chaos. Indeed, it has also been shown that a stationary probability association occurs for strong chaos and a non-stationary probability association occurs for weak chaos. However, it should be noted that investigation of non-stationary feature of probability association based on experiment is still scant. In our experimental results, the non-stationary characteristics persisted at the transition between the RO state and the RCB state. This feature can be well reproduced by the numerical simulation of complicated L-K equations with strong phase fluctuation. The finding reported (experimental as well as numerical) here should be of interest to nonlinear dynamics. Indeed, we have seen that the onset of new statistics (*i.e.*, non-stationary characteristics) strongly related to some physical characteristics, *i.e.*, chaotic spiking. Finally, the characterization of Lyapunov exponent based on experimental time series is also an important work and it is on progress as the future work.

The work of the NCKU group is partially supported by the National Science Council, Taiwan, ROC under project Nos. NSC88-2112-M-006-001 and NSC89-2112-M-006-023. This research of K.O. was in part supported by Monbusho International Scientific Research Program: Joint Research 10044175. We are indebted to S.-L Hwong, J.-Y. Ko, and A.-C. Hsu for discussions.

References

1. A. Lasota, M.C. Mackey, *Chaos, fractals, and noise*, 2nd edn. (Springer-Verlag, New York, 1994).
2. H. Kantz, T. Schreiber, *Nonlinear time series analysis* (Cambridge Univ. Press, New York, 1997).
3. H.G. Schuster, *Deterministic chaos: an introduction* (VCH, New York, 1995).
4. J.-L. Chern, T.C. Chow, Phys. Lett. A **192**, 34 (1994); J.-L. Chern, F.-J. Kao, I.-M. Jiang, *ibid.* **218**, 268 (1996);
5. S. Parthasarathy, S. Rajasekar, Phys. Rev. E **58**, 6839 (1998).
6. R.M. May, Nature **261**, 459 (1976); M.C. Mackay, L. Glass, Science **197**, 287 (1977); J. Foss, A. Longtin, B. Mensour, J. Milton, Phys. Rev. Lett. **76**, 708 (1996); K. Ikeda, Opt. Commun. **30**, 257 (1979).
7. T. Sano, Phys. Rev. A **50**, 2719 (1994).
8. J. Sacher, W. Elsässer, E.O. Göbel, Phys. Rev. Lett. **63**, 2224 (1989).
9. I. Fischer, G.H.M. van Tartwijk, A.M. Levine, W. Elsässer, E.O. Göbel, D. Lenstra, Phys. Rev. Lett. **76**, 220 (1996).
10. B. Meziane, P. Besnard, G.M. Stephan, IEEE J. Quant. Electron. **31**, 617 (1995).
11. K. Otsuka, Appl. Opt. **33**, 1111 (1994).
12. K. Otsuka, Appl. Phys. **18**, 415 (1979); IEEE J. Quant. Electron. **QE-15**, 655 (1979).
13. K. Otsuka, J.-Y. Ko, J.-L. Chern, K. Ohki, H. Utsu, Phys. Rev. A **60**, R3389 (1999).
14. G.P. Agrawal, N.K. Dutta, *Semiconductor Lasers*, 2nd edn. (Van Norstrand Reinhold, New York, 1993).
15. J.-S. Lih, J.-Y. Ko, J.-L. Chern, I.-M. Jiang, Europhys. Lett. **40**, 7 (1997).
16. R. Lang, K. Kobayashi, IEEE J. Quant. Electron. **QE-16**, 347 (1980).
17. M. Lax, Rev. Mod. Phys. **32**, 25 (1960); **38**, 541 (1966); Phys. Rev. **160**, 290 (1967); Phys. Rev. **157**, 231 (1967); M. Lax, W.H. Louisell, Phys. Rev. **185**, 568 (1969).
18. J.-L. Chern, T.-C. Hsiao, J.-S. Lih, L.-E. Li, K. Otsuka, Chin. J. Phys. **36**, 667 (1998).
19. W.H. Press, S.A. Tenkolsky, W.T. Vettering, B.P. Flannery, *Numerical recipes in Fortran: the art of scientific computing*, 2nd edn. (Cambridge Univ. Press, Cambridge, 1992), p. 614.
20. K. Otsuka, Y. Asakawa, R. Kawai, S.-L. Hwong, J.-L. Chern, Jpn J. Appl. Phys. **37**, L1523 (1998); K. Otsuka, H. Utsu, R. Kawai, K. Ohki, Y. Asakawa, S.-L. Hwong, J.-Y. Ko, J.-L. Chern, *ibid.* **38**, L1025 (1999).